J Appl Electrochem (2016) 46:539–549
DOI 10.1007/s10800-016-0943-3

RESEARCH ARTICLE

On the use of atomic force microscopy and scaling analysis to quantify the roughness of zinc electrodeposits produced from an industrial acid sulfate electrolyte containing glue

Said Sharif Mahboob[1] · **Kirsten Swanson**[1] · **Jose Alberto Gonzalez**[2] · **Jeffrey L. Shepherd**[1]

Received: 29 September 2015 / Accepted: 27 January 2016 / Published online: 8 February 2016

Abstract The morphology and roughness of zinc electrodeposits produced on an aluminum cathode from an industrial acid sulfate electrolyte have been characterized with scanning electron microscopy (SEM), atomic force microscopy (AFM), and scaling analysis. SEM and AFM images provided a topographical view of the deposit, while scaling analysis was used to determine the mechanism of surface growth and to quantify surface characteristics including the root-mean-squared (*rms*) roughness and periodicity. For an electrolyte with a fixed composition of additives, both the *rms* roughness and the width of the surface features increased with deposition time and the mechanism of surface growth was dominated by surface diffusion. However, when the deposition time was fixed but the concentration of glue in the electrolyte was increased between 3 and 60 mg L^{-1}, a marked change in the deposition mechanism was observed. Here, small elevations in glue had minimal influence on the *rms* roughness but reduced the width of surface features thereby producing rougher deposits. At glue concentrations above 30 mg L^{-1}, the scaling analysis plot changed considerably and corresponded to samples with two distinct deposit morphologies on a single surface, an observation that was not apparent from the SEM images alone. The features include large zinc islands with numerous small zinc features on their surfaces, which indicate competing mechanisms of nucleation and surface diffusion, respectively. The results show that scaling analysis offers complementary information to SEM characterization and can render additional information on the mechanism of zinc deposition under industrial conditions.

Graphical Abstract

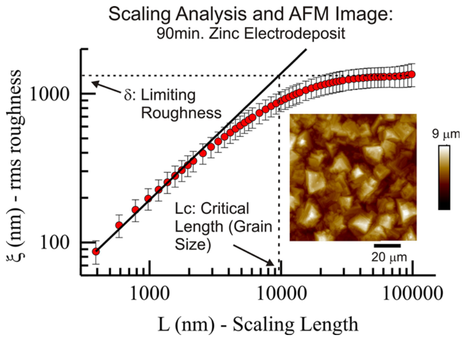

Keywords Zinc electrowinning · Atomic force microscopy (AFM) · Scaling analysis · Bone glue additive · Surface roughness leveling

1 Introduction

The electrowinning of zinc onto a cathode material is a critical stage of industrial zinc production and it is desirable for this process to occur at high current densities while rendering level and uniform zinc deposits [1] that can be easily stripped from the cathode substrate [2]. In practice, zinc can be electrodeposited from different electrolytes (industrial and non-industrial) and onto a variety of cathodes [3–8] and the characteristics of deposition can be influenced by factors including electrolyte concentration

---

✉ Jeffrey L. Shepherd
jshepherd@laurentian.ca

[1] Department of Chemistry and Biochemistry, Laurentian University, Sudbury, ON P3E 2C6, Canada

[2] Applied Research and Technology Group, Teck Metals Ltd., Trail, BC V1R 1S4, Canada

and composition [9–21], electrolyte impurities [22–25], current density and temperature [26, 27], as well as pH [28]. These factors may affect the morphology and roughness of a zinc deposit and are important considerations for the operating practices of a zinc production plant. During industrial electrowinning of zinc, the deposition occurs onto an aluminum cathode at high current densities (~470 A m^{-2}) from an acidic zinc sulfate solution that is modified to contain a host of additives [29]. For instance, the electrolyte may contain additives including licorice (an acid mist suppressor), strontium carbonate (to remove solubilized lead), antimony and sodium silicate (to refine grain size), as well as glue (a leveling agent) [29]. As such, the composition of an industrial zinc electrolyte may be complex and maintaining a uniform electrolyte throughout the tankhouse is an important component in producing uniform zinc deposits. Even with the inclusion of additives, a zinc deposit may still grow unevenly and make contact with the anode in the electrochemical cell. These events, although minimized by the action of the additives, result in production losses within the plant and short-circuits remain a problem during industrial zinc deposition. In this regard, the morphology and growth characteristics of zinc deposits produced in an industrial setting require further study.

There are numerous studies that have characterized a wide range of zinc deposits using high-resolution surface probes. For example, zinc deposits produced on various substrates and from different electrolytes have been widely characterized with SEM [2, 7, 8, 10, 15, 16, 18, 19, 21, 22, 24, 26, 30–34] to gain insight into the morphological structure of surfaces under different deposition parameters. Zinc deposits have also been studied with 3-dimensional techniques such as AFM [4, 13, 33–35] which not only offer a topographical view of the surface but can also be used to quantify roughness properties such as the *rms* variation of surface heights. While this parameter is useful in quantifying roughness, the *rms* value only describes variations in the vertical direction of the surface and does not completely describe the overall roughness characteristics. The periodicity of surface features (or corrugation) should also be considered. With these two parameters one can determine the aspect ratio of surface features and therefore quantify the general roughness properties more accurately. In fact, the surface with the higher aspect ratio for a given *rms* roughness should be considered the rougher sample [36]. The corrugation of a surface may be obtained through cross-sectional analysis of a 3-dimensional image but this approach only analyses a portion of the image. A method that samples the entire surface is beneficial and may be achieved through the mathematical approach of scaling analysis, which can extract surface growth parameters including the limiting roughness (δ) and periodicity (L_C, critical length) which are related to the aspect ratio through δ/L_C [37]. Moreover, scaling analysis can also be used to extract the mechanism of surface growth, allowing one to determine the dominant roughening/smoothing processes [36, 37].

Scaling analysis has been applied to study the surface characteristics of electrodeposited copper [37–39] and some studies have also been performed on zinc. For example, scaling analysis has been used to characterize a Ni–Zn binary alloy electrodeposit [40] or a pure zinc deposit on a copper cathode [41]; yet the application of scaling theory to characterize pure zinc deposits on an aluminum cathode from an industrial acidic electrolyte has been understudied. In fact, the majority of high-resolution probe studies on industrially produced zinc deposits have focussed on SEM characterization [1, 30, 31]. These studies, among others, have shown that zinc generally deposits onto the aluminum cathode in platelets with a characteristic orientation and crystal geometry that is dependent on the current efficiency and electrolyte purity [22]. While many important aspects of industrial zinc deposits have been previously described, scaling theory may add further quantification of these important surfaces and give insight into the deposition mechanisms. In this paper, AFM and scaling analysis are used to characterize zinc deposits produced on an aluminum cathode from an industrial electrolyte with a composition similar to that used in a zinc electrowinning plant. The approach is similar to previous studies that have used SEM to characterize the influence of both deposition time and additions of glue on the structure and morphology of industrial zinc deposits on aluminum cathodes [1, 30, 31]. The influence of glue and deposition time on industrial zinc deposition are further characterized in this report by making use of scaling analysis to quantify the surface growth characteristics.

2 Experimental

2.1 Electrolyte

The electrolyte was prepared using a purified neutral zinc solution containing 168 g L^{-1} zinc and was provided by Teck. A typical composition of this neutral feed can be found in a recently published survey of plant operating data [29]. The neutral feed was adjusted with H_2SO_4 (Sigma-Aldrich, 98 %) and ultrapure water (Milli-Q, Synergy UV, 18.2 MΩ cm) to achieve a concentration of 160 g L^{-1} H_2SO_4 and 60 g L^{-1} Zn. This solution was further adjusted to contain 9 mg L^{-1} of licorice (supplied by Teck) and 2.7 mg L^{-1} of sodium silicate (Sigma-Aldrich). In this paper, an electrolyte with the above composition is referred to as the *standard electrolyte* which was further modified with various levels of glue (supplied by Teck) as reported in the body of the paper. The glue additions were at 3, 7.5, 15, 22.5, 30, 37.5, and 60 mg L^{-1}. The electrolytes were prepared fresh for each trial to avoid degradation of the additives. Furthermore, the electrolyte was always prepared using analytical glassware that was first cleaned in a heated acid bath mixture composed of 50:50 (v:v) concentrated sulfuric and nitric acid. After cleaning, the glassware was thoroughly rinsed with ultrapure water before solutions were prepared.

2.2 Electrochemical procedure

All zinc deposits were produced at room temperature in an electrochemical cell containing an aluminum cathode (provided by Teck) and a platinum anode (Alfa Aesar, 1 mm diam. 99.99 %). Although the anode used in the industrial setting is typically a lead-silver anode, a platinum electrode was used to avoid lead contamination in the electrolyte in a manner similar to that previously reported [30]. The aluminum cathode was cut into a 1 cm × 1 cm square and a steel wire was pressed against the back of the sample to make electrical contact. Both the aluminum and steel wire were fully encased in an epoxy (LECO—Resin epoxy and hardener) and only the front face of the aluminum cathode was exposed by sanding with 180, 280, 400, and 600 grit sandpaper after the epoxy had cured. The aluminum surface was further polished to a mirror finish with 6, 3, and 1 µm of water-based diamond suspensions (BUEHLER). This procedure resulted in the cathode having a uniform polished surface with a known geometric area of 1 cm^2. The aluminum sample was polished with the 1 µm diamond suspension after each electrodeposit was peeled from the substrate. The anode was fashioned by shaping a 5 cm length of the platinum wire into a loop to create a geometric area of 1.6 cm^2. This area was chosen because it provides a cathode/anode area ratio that is similar to what can be achieved in the AFM electrochemical cell. Although no in situ AFM studies are discussed in this report, the cathode/anode area was maintained for comparison with potential in situ studies in the future.

To perform electrodeposition, the two electrodes were positioned at a distance of 0.5 cm from each other and were simultaneously placed in the cell containing the freshly prepared electrolyte. Zinc was deposited by maintaining a cathodic current density of 44 mA cm^{-2} using a potentiostat (Pine model AFRDE5 Bi-Potentiostat) operating in galvanostatic mode and the current was controlled by in-house software written in LabVIEW. Electrodeposition was performed over 10, 30, 50, 70, or 90 min at which point the electrodes were immediately removed from the cell and rinsed in ultrapure water to avoid dissolution of the zinc deposit back into the acidic electrolyte. The zinc sample was then peeled off the cathode using tweezers and placed on a Kimwipe® to dry. A total of 3 samples were independently produced for each deposition time and/or electrolyte composition and the electrolyte was routinely prepared for each. These samples represent 3 independent trials for each deposition condition. Once the samples were dry, they were weighed and mounted on a sample holder for either SEM or AFM imaging.

2.3 SEM imaging

All SEM images were acquired using a JEOL 6400 scanning electron microscope. The instrument was operated at an accelerating voltage of 20 kV and a beam current of 1 nA and the vacuum chamber was maintained at approximately 10^{-6} mbar. The samples received no surface cleaning or additional treatment before SEM imaging.

2.4 AFM imaging

AFM images were acquired on a Bruker Instruments Nanoscope 3D Multimode Atomic Force Microscope operating in tapping mode. The cantilever probe (Bruker Probes, TESPA) had a nominal frequency of 320 kHz and a force constant of 42 N m^{-1}. Each image was acquired with a size of 100 µm × 100 µm and a resolution of 0.1953 µm/pixel. The image scan frequency was between 0.3 and 0.5 Hz and the offline plane fit was engaged. Every sample was imaged at 3 different and random positions on the surface. These three images represent triplicate analysis for one deposit condition. Given that there were 3 trials for each deposit, this results in a total of 9 AFM images per deposit condition. To improve the visual representation of the AFM images in this paper, the files were sometimes cropped or contrast-enhanced using Bruker Nanoscope software. However, scaling analysis was only performed on the raw AFM images that received no additional processing after their acquisition. To perform scaling analysis, the surface heights of the raw AFM image were exported as ASCII files using the Nanoscope software. The ACSII files were imported into a MATLAB program and used to calculate the scaling analysis as described in the next section.

2.5 Scaling analysis

In scaling analysis, the *rms* roughness (ξ) of a surface is calculated over different scale lengths (L) of the image. This is accomplished using the following equation [36, 37, 42, 43]:

$$\xi(L,t) = \sqrt{\langle [H(r,t) - \langle H(r,t)\rangle]^2\rangle}. \quad (1)$$

Here t represents time, H represents height, and < > is the spatial average over a position r on the surface. This equation was applied to the AFM data using a MATLAB algorithm that was written in-house. Briefly, the *rms* value was calculated within all possible 2 × 2 pixel arrays in the raw image and their average represents the *rms* roughness (ξ) at a defined scaling length. For our images, a 2 × 2 pixel array corresponds to a scaling length of $L = 390$ nm. The calculation was then repeated for all possible 3 × 3 pixel arrays in the image ($L = 586$ nm) and the data were again averaged to provide a new ξ at the larger scaling length. This process was repeated with increasing pixel array sizes until the maximum scaling length (i.e., the total image size) was achieved. In this study, the size of the pixel array was increased by a value of 1 for the first 10 calculations of ξ and then by a value of 2, 4, 8, 16, and 32 for each subsequent cluster of 10 ξ calculations. The data are viewed by plotting log ξ versus log L and various parameters are extracted from these plots as described in the results and discussion section.

3 Results and discussion

3.1 Comparison of zinc structures using AFM and SEM

The typical structure of a zinc electrodeposit is presented in Fig. 1 and the images were acquired from (a) SEM, (b) AFM top view, and (c) AFM 3D view. The zinc sample presented in Fig. 1 was produced from a 30-min deposit using the standard electrolyte containing 3 mg L^{-1} of glue. In the SEM image (Fig. 1a), the deposit takes the morphology of zinc platelets that are characteristic of samples produced from this type of industrial electrolyte containing a low concentration of glue [22] and confirms that zinc deposits produced in this study match the structure of those prepared under similar conditions. Furthermore, the SEM image can be directly compared with the AFM image shown in Fig. 1b. This image was taken from the same sample but over a different region of the surface. On comparison, it is apparent that the general size, shape, and distribution of the surface features are similar between the two imaging methods showing that the tip probe of the AFM does not induce artifacts or distort the zinc surface characteristics. This ensures that the AFM image is an accurate representation of the zinc surface and therefore offers reliable height information. As shown in the color bar of Fig. 1b, the variations in surface heights can range from a few to several micrometers. This is further visualized in Fig. 1c which is a 3-dimensional representation of the sample. This 3D image shows numerous features on the surface with a distribution of both surface heights and corrugation. Analysis of the AFM image may then be used to accurately quantify the surface roughness characteristics and is demonstrated with the application of scaling analysis.

3.2 Scaling analysis of zinc deposits produced at different deposition times

To demonstrate the application of scaling analysis, a series of zinc deposits were produced at deposition times of 10, 30, 50, 70, and 90 min from the standard electrolyte containing 30 mg L^{-1} of glue. The results for the 10- and 90-min deposits are presented in Fig. 2a, and the error bars represent the standard deviation of 3 independent trials (NB: the data for each trial are an average from the triplicate analysis discussed in Sect. 2.4). Scaling analysis was also conducted on the 30-, 50-, and 70-min deposits and show similar trends; however, they were excluded from Fig. 2a for image clarity.

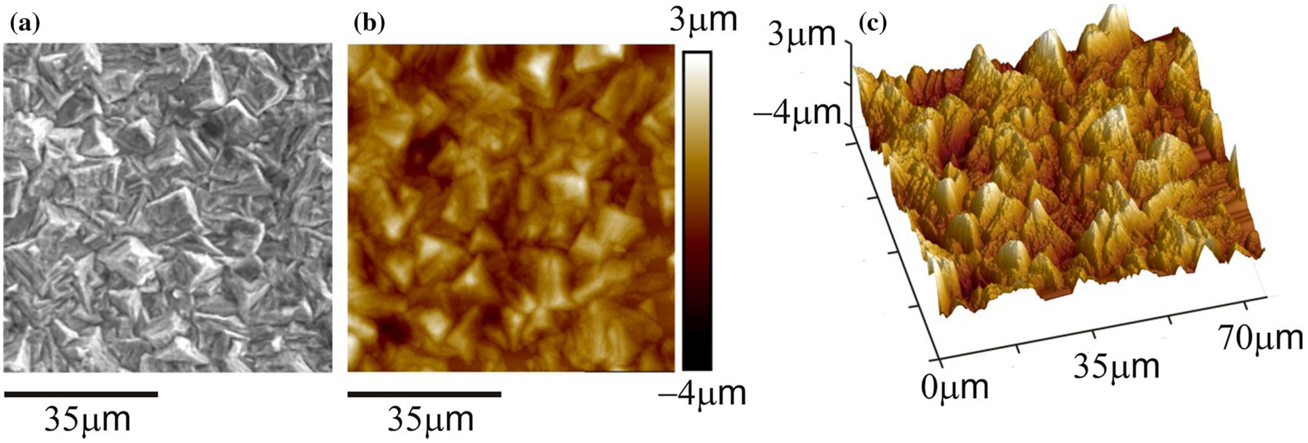

Fig. 1 **a** SEM, **b** AFM (*top view*) and **c** AFM (*3D view*) images of a zinc deposit produced on an aluminum cathode after 30 min of deposition at a current density of 44 mA cm^{-2}. This deposit was prepared from the standard electrolyte containing 3 mg L^{-1} of glue. All images were cropped to a scale of 75 μm in width and height for direct comparison

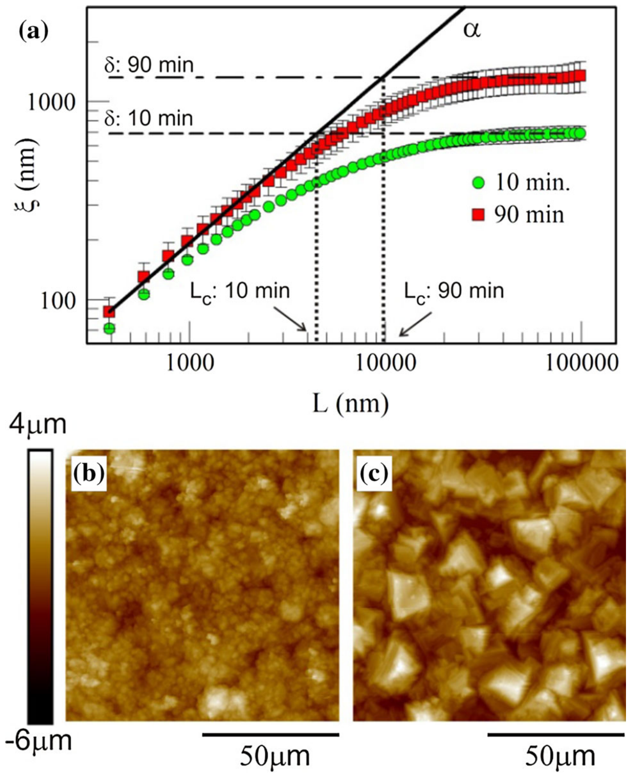

Fig. 2 A representation of **a** scaling analysis and **b**, **c** AFM images independently obtained for zinc deposits produced on an aluminum cathode after **b** 10 and **c** 90 min of deposition using a current density of 44 mA cm^{-2}. The deposits were produced from the standard electrolyte containing 30 mg L^{-1} glue. In **a** the log ξ versus log L plot shows where various scaling parameters can be extracted including the static exponent (α), limiting roughness (δ), and the critical scaling length (L_C). The *error bars* represent the standard deviation of 3 independent trials for each deposit time

Both trends shown in Fig. 2a match the general characteristics predicted by scaling theory and show features that are consistent with the scaling analysis of other metal deposits [36, 37, 39, 41]. For instance, at low values of L, scaling theory predicts [36]

$$\xi \propto L^{\alpha} \quad \text{for} \quad L \ll L_C, \tag{2}$$

where L_C represents a critical length. Over these small scaling lengths, a plot of log ξ versus log L shows a linear trend with a slope that corresponds to the static (or spatial) exponent (α) which can be used to make a statement about a growth mechanism [36, 37, 39, 41]. Typically, the growth of an electrodeposit can be viewed as a balance between stochastic roughening and a smoothing mechanism. The static exponent can be used in the relation $n = 2(\alpha + 1)$ [36] and a value of $n = 4$ indicates that deposition is controlled by surface diffusion but $n = 3$ indicates that smoothing is controlled by volume or bulk diffusion. Surfaces that are uniformly self-similar are characterized by a value of $\alpha = 1$, whereas self-affine surfaces have static exponents that typically range between 0 and 1. Since the static exponent should be independent of electrodeposition time [36, 37], it was extracted by globally fitting a straight line to the first 7 data points of all scaling analysis plots (i.e., globally for the 10, 30, 50, 70, and 90 min. datasets). This fitting rendered the straight line in Fig. 2a and a value of $\alpha = 0.85$, which gives $n = 3.7$. This shows that zinc deposited onto aluminum from the standard electrolyte containing 30 mg L^{-1} of glue produces a self-affine surface and that the growth is controlled by surface diffusion. However, it is emphasized that this deposit was produced over 30 min of deposition in contrast to the industrial practice that harvests zinc after 24 h [29]. In this regard, the analysis of a zinc deposit produced from a longer deposition time is desirable but the roughness of such a surface would be outside the operating parameters of the AFM. This limits the use of AFM in the analysis of longer deposits; however, the temporal properties of the surfaces can be predicted with scaling analysis if the dynamic exponent (β) is known. This has been shown with industrially relevant copper electrodeposits and the predicted roughness shows a remarkable agreement with the value measured using White Light Interference Microscopy [37].

The dynamic exponent can be extracted using a set of scaling data at large L. As shown in Fig. 2a, the plot of log ξ versus log L shows a plateau at large-scale lengths because the roughness eventually becomes independent of L. At this point, the surface has attained a characteristic limiting roughness ($\xi = \delta$) which can be determined by extrapolating the plateau to the y-axis. This is shown by the two dashed lines in Fig. 2a and reveals that the limiting roughness is a function of deposition time for which scaling theory predicts [36]:

$$\delta \propto t^{\beta} \quad \text{for} \quad L \gg L_C. \tag{3}$$

The dynamic (or temporal) exponent (β) can be determined from a separate plot of log δ versus log t. This exponent can be used in conjunction with α to determine the mechanism of growth but Eq. 3 can also be used to predict the limiting roughness of a surface after a prolonged deposition time.

Both of the static and dynamic exponents are important parameters to describe the scaling characteristics of surfaces and they can be predicted with theory [36]. However, the parameters δ and L_C, which describe the limiting roughness and critical scaling length, are system dependent. The limiting roughness has already been discussed but the critical scaling length represents the point (or length) at which the *rms* roughness achieves the limiting value and may be regarded as the corrugation or periodicity of the surface features. The critical point, L_C, is extracted at the intersection of the α-line and the δ-line as shown by the dotted trends in Fig. 2a. The 10-min deposit has a smaller value of L_C compared to the 90-min deposit. This indicates that the width (or grain size) of the surface features are increasing as the deposition of zinc continues with time. This is visually apparent when looking at the AFM images in Fig. 2b, c which represent zinc deposits produced separately at 10 and 90 min, respectively. After 10 min of deposition, the AFM image is characterized by many features that have a small width and they cover the surface fairly uniformly. However, after 90 min of deposition, the AFM image shows that the surface features have grown to a significantly larger width. Scaling theory accounts for this through the equation [36]:

$$L_C \propto t^{\beta/\alpha} \qquad (4)$$

which allows one to predict the periodicity of a deposit produced over a longer deposition time.

In all, scaling analysis is not only useful in extracting the static and dynamic exponents but it may also be used to quantify and predict the surface characteristics such as periodicity and limiting roughness of the industrially produced zinc deposits. This quantification is important because visual inspection of zinc deposits or their images alone may not accurately describe the relative changes of roughness to periodicity. For instance, the time-dependent variation in surface roughness and periodicity can be visually observed by the set of AFM images presented in Fig. 3. Each AFM image shown was obtained from an independent sample produced at (a) 10, (b) 30, (c) 50, (d) 70, and (e) 90 min of deposition from the standard electrolyte containing 30 mg L^{-1} of glue. All of the axes are held at a constant value so that the height and width of surface features can be directly compared between each image. The images were originally 100 μm in size but were cropped to 50 μm to enhance subtle differences. On inspection of Fig. 3, some trends can be observed. Firstly, the *rms* roughness shows a general increase from image a) to e) as the fluctuations in the surface heights become larger with the increased deposition time. Also, there is a general increase in the average width of the surface features as the deposition time increases. As such, one would expect increasing values of δ and L_C as a function of time. However, the rate at which the surface roughness changes relative to the periodicity is not apparent from visual inspection alone. This relative change can be quantified by analysis of δ and L_C as a function of time as shown in Fig. 4.

The stack plot in Fig. 4 shows the average distributions of (a) δ, (b) L_C, and (c) δ/L_C for all of the zinc deposits produced as a function of time from the standard electrolyte containing 30 mg L^{-1} of glue. The data were extracted from the scaling analysis previously described in Fig. 1a (which only presented the data for 10 and 90 min)

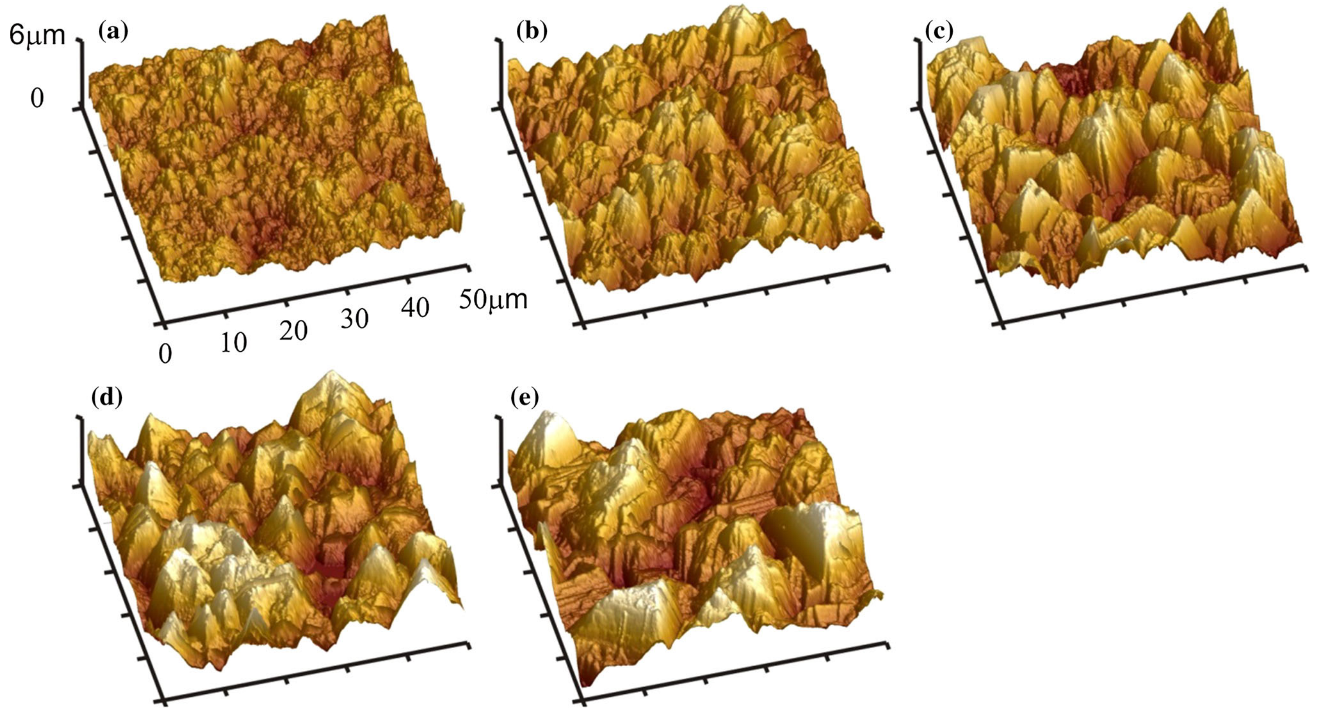

Fig. 3 AFM images produced after **a** 10, **b** 30, **c** 50, **d** 70, and **e** 90 min of zinc deposition onto an aluminum cathode using a current density of 44 mA cm^{-2}. These deposits were independently produced from the standard electrolyte that contained 30 mg L^{-1} of glue. The images represent only one from each trial and were initially 100 μm in length. Each image was subsequently cropped to show the visual changes more clearly. The *x*- and *y*-axes are 50 μm in length for all images but are presented only on (**a**) to reduce image clutter

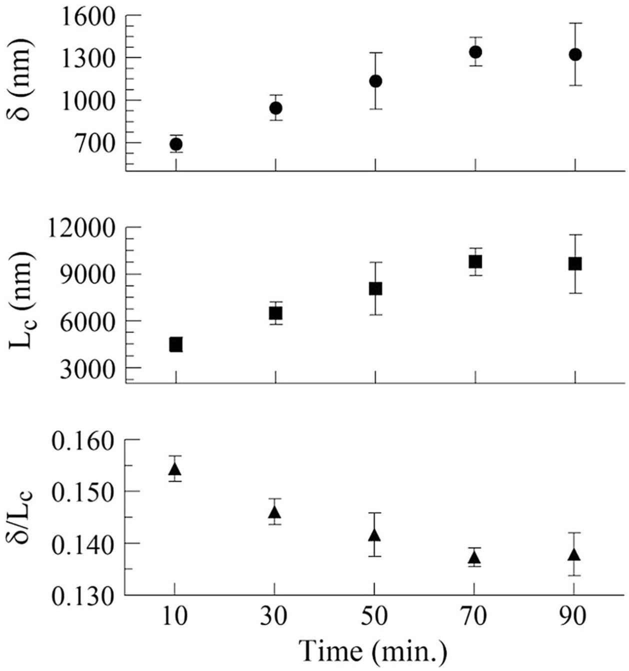

Fig. 4 Analysis of **a** δ, **b** L_C, and **c** δ/L_C for zinc deposits produced over a range of deposition times. The electrolyte and deposition conditions are the same as those described in Fig. 3. Each data point was extracted from the log ξ versus log L plots of three independent trials and the *error bars* represent the standard deviation of this analysis

using a value of $\alpha = 0.85$. The error bars in Fig. 4 represent the standard deviation of three independent trials for each deposition time. In Fig. 4a, b, a clear increase in the limiting roughness and critical length are observed. This is in agreement with the visual inspection of the AFM images presented in Fig. 3 although there is not a significant difference between the limiting roughness of the 70- and 90-min deposits. This could be related to the operating limit of the AFM as some images produced at 90 min would occasionally show features that were saturated in height. Because of this limitation, deposition times longer than 90 min were not studied. While there is also some variability in the data at 50 min, there is clear separation in the error bars between the 10- and 90-min datasets showing that the increasing trend is statistically significant. Therefore, it is concluded that both δ and L_C are increasing as a function of deposition time. The limiting roughness data presented in Fig. 4a were used with Eq. 3 to extract a dynamic exponent of $\beta = 0.31$ and is again in support of a smoothing mechanism dominated by surface diffusion [36]. The dynamic exponent was also used in Eqs. 3 and 4 to predict the limiting roughness and periodicity of samples produced after longer deposition times. The results predict values of $\delta \sim 4$ µm and $L_C \sim 36$ µm for zinc samples produced on aluminum after 48 h of deposition from the standard electrolyte containing 30 mg L^{-1} of glue.

The relative changes between δ and L_C are shown in Fig. 4c. Here the ratio of δ/L_C shows an inverse relationship with deposition time and suggests that the surface is becoming smoother. This occurs because the width of surface features are increasing at a more rapid rate than the *rms* roughness and this anisotropic growth is a feature expected for a self-affine surface [36]. From these combined observations, it is concluded that the growth of these industrially relevant zinc deposits is governed by a competition between stochastic roughening and a smoothing mechanism involving surface diffusion. However, it is emphasized that these deposits were produced under strictly controlled conditions using a polished aluminum cathode, a platinum anode, an industrial acid zinc sulfate solution containing 30 mg L^{-1} of glue and a current density of 44 mA cm^{-2} at room temperature. Variations in these parameters could influence the features of deposition. This was explored in a study where the deposition time was held constant at 30 min but the composition of glue was varied.

3.3 Influence of glue additions on the surface characteristics of zinc deposits

In this section, scaling analysis was used to investigate the influence of glue additions on the morphology of zinc deposits. The influence of animal glue on the leveling of electrowon copper [44] and other metals has been previously investigated [45] and a mechanism of smoothing has been proposed. Animal glue is a protein colloid that is positively charged and it is believed to adsorb to the negatively charged protrusions on the surface because they carry a locally high current density. Once adsorbed, the insulating behavior of bone glue allows for metal deposition to occur in lower recesses of the surface which have lower current densities. This action of smoothing is consistent with the observations above that showed a surface periodicity increasing faster than the surface limiting roughness. This mechanism could have occurred due to the presence of glue in the electrolyte at a concentration of 30 mg L^{-1}. However, variations in the glue concentration may show differences in the smoothing mechanism that may be manifested by changes in the surface roughness characteristics including the static exponent α. To explore this possibility, a series of zinc deposits were produced from the standard electrolyte but with variations in the level of glue to 3, 7.5, 15, 22.5, 30, 37.5, and 60 mg L^{-1}. These deposits were created independently and in a random order to avoid any systematic errors. For each deposit, the current density was 44 mA cm^{-2} and only one deposition time of 30 min was studied. Because the value of α may change with glue concentration, the static exponent was not determined from a global fit of the data for all glue concentrations. Rather, the value of α was determined for each glue composition independently by fitting a straight line to the first 7 data points of the log ξ versus log L plots of the 3 trials for each glue level. A portion of the results are presented in Fig. 5 which compares the scaling analysis and AFM/SEM images for selected deposit conditions.

Figure 5a shows the AFM image (left), SEM image (right), and scaling analysis (bottom) obtained for a deposit prepared from the standard electrolyte containing 7.5 mg L^{-1} of glue. The AFM and SEM images show features that are comparable to each other and are composed of zinc deposits arranged in platelets across the surface. These general observations are consistent with the data presented in Fig. 1 and the general features of the scaling analysis are consistent with that previously described in Fig. 2a (although the values of δ and L_C are different as further described Fig. 6). In Fig. 5b, the concentration of glue was elevated to 22.5 mg L^{-1} and some subtle differences are noticed. For instance, the AFM and SEM images are again comparable to each other in that they both reveal the typical zinc platelet structure. However, the size/width of the features has decreased when the level of glue is elevated from 7.5 to 22.5 mg L^{-1}. This is visually noted when comparing the AFM and SEM images in Fig. 5b with those in Fig. 5a. A similar comparison of the respective scaling analysis plots shows that L_C has shifted to a lower value with the elevated glue concentration. This suggests that increasing levels of glue produce smaller grains on the surface, at least for these 30-min deposits. This reduction in grain size continues as more glue is added to the electrolyte but at a critical point, the surface begins to show more unique morphologies. This is apparent in Fig. 5c which represents the data for a zinc deposit produced from the standard electrolyte containing 37.5 mg L^{-1} of glue. Here the AFM image shows two distinct deposit morphologies on a single surface. These appear to be small zinc platelets on the surface of a larger underlying zinc feature. This is an interesting observation and is not as clearly represented in the SEM image alone. While the small features can be observed in the SEM image, the larger background features are only subtly noted and appear as rolling hills or small waves in the background. Industrial zinc deposits produced on aluminum cathodes and high glue concentrations (50 mg L^{-1}) have been previously characterized with SEM and the deposit morphologies do show a general reduction in grain size [30]. In these previous reports, the surface features are comparable to the small features seen in the AFM and SEM images presented in Fig. 5c. However, the larger underlying features were not apparent in that previous study. Other reports have described a vertical morphology of the zinc platelets at high glue concentrations [1, 22], although the latter reference used a Pb–Ag anode and the structure may

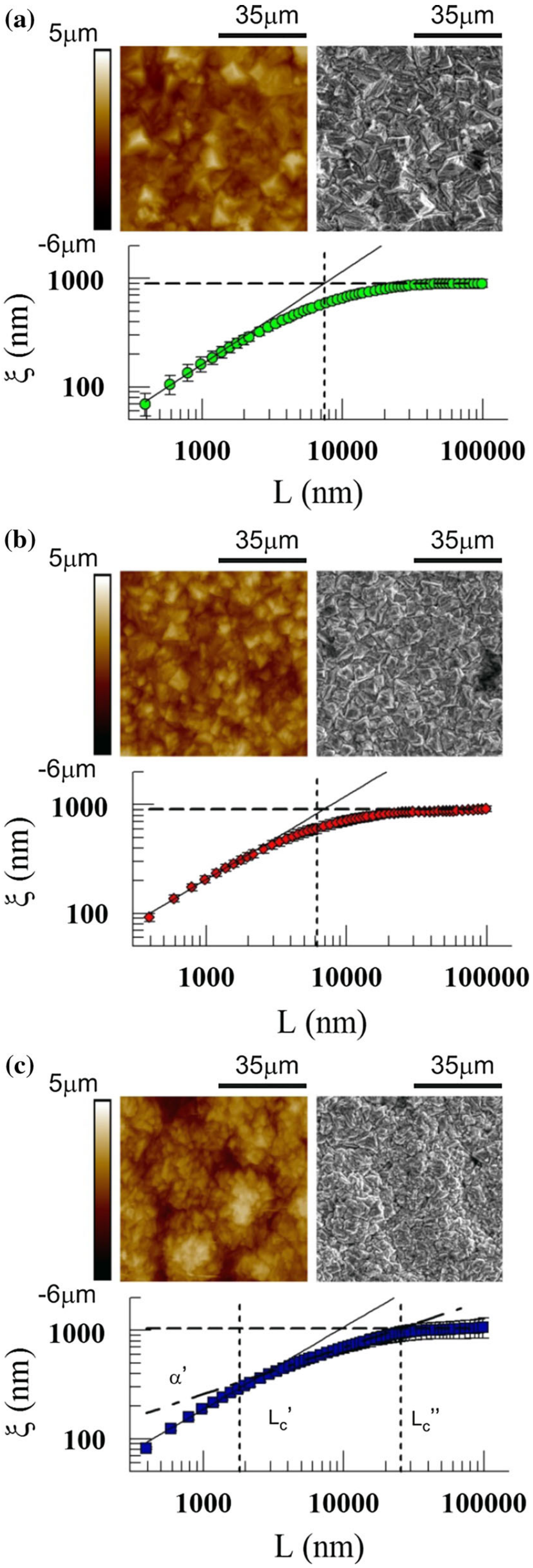

Fig. 5 Comparison of zinc deposits produced on an aluminum cathode at 44 mA cm^{-2} from the standard electrolyte containing **a** 7.5, **b** 22.5, and **c** 37.5 mg L^{-1} of glue. In *each panel*, the AFM image is presented at the *top left* and the SEM image at the *top right*. Beneath these images are the log ξ versus log L plots for each deposit condition. The *error bars* represent the standard deviation of three trials

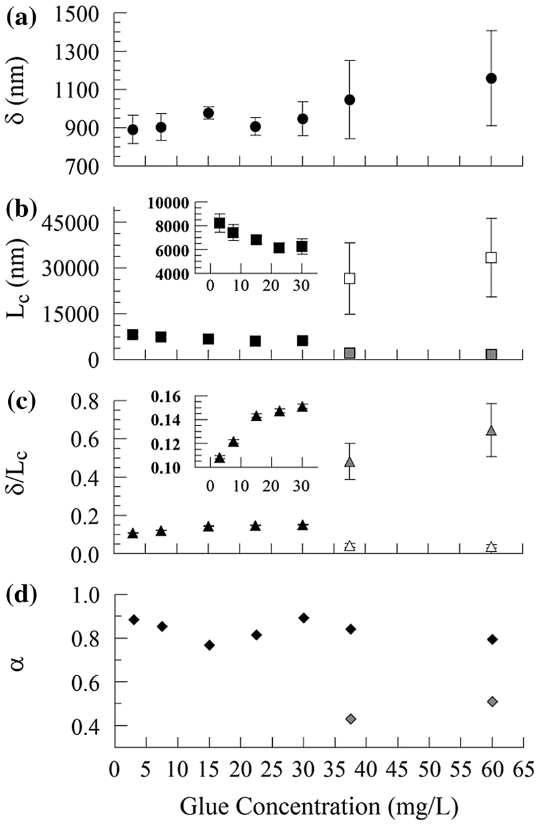

Fig. 6 Analysis of **a** δ, **b** L_C, **c** δ/L_C, and **d** α for zinc deposits produced on an aluminum cathode at 44 mA cm^{-2} and one deposition time of 30 min. The standard electrolyte was used but contained a range of glue concentrations as indicated on the *x*-axis. Each data point was extracted from the log ξ versus log L plots of three independent trials and the *error bars* represent the standard deviation of this analysis. Data with a *gray* shading represent a parameter designated with a prime and *open symbols* represent a parameter designated with a double prime. In **b** and **c**, the *inset* represents an expanded view of the data between 3 and 30 mg L^{-1} of glue

be related to lead impurities in the electrolyte. As such, the large underlying zinc features deserve further description, especially since the samples with this structure produce more distinct scaling features and a new type of growth mechanism. The distinguishing feature of the scaling analysis is the second linear region in the log ξ versus log L plot at intermediate scaling lengths. At low L, the scaling analysis plots shows the familiar linear region and, at a characteristic crossover length (L_C'), a new linear region is established with a new static exponent (α'). These scaling features have been observed on different surfaces [40, 46, 47] and the origin of the crossover can be related to the size and shape of different grains on the surface [46, 47]. By treating L_C' as the periodicity of the smaller features and L_C'' as the periodicity of the larger features, the relative grain sizes can be extracted. Moreover, by extracting the different values of α and α', new insight can be gained about the deposition mechanism. This is most clearly described by comparing the scaling parameters for the whole range of glue concentrations studied and is described in Fig. 6.

The stack plot in Fig. 6 shows the distribution of (a) δ, (b) L_C, (c) δ/L_C, and (d) α for the 30-min zinc deposits produced from the standard electrolyte containing a range of glue concentrations. The data were extracted from scaling analysis plots and again, the error bars represent the standard deviation of three independent trials for each deposit condition. The limiting roughness shown in Fig. 6a has no clear trend within the set of glue concentrations studied. In fact, all of the error bars in the dataset overlap to some extent and indicate that the limiting roughness is not changing significantly for these 30-min deposits as the level of glue increases. However, there are clear changes in the periodicity as shown in Fig. 6b. Here, the black squares represent L_C, while the gray and open squares represent L_C' and L_C'', respectively. To show trends in the data more clearly, the values of L_C are expanded in the inset which reveals a decreasing periodicity as the glue concentration is elevated between 3 and 30 mg L^{-1}. Although there is some overlap in the error bars, there is a clear separation of data between 3 and 30 mg L^{-1} indicating that the data points are, in fact, significantly different. At glue concentrations of 37.5 and 60 mg L^{-1}, two zinc deposit morphologies are manifested in the graph. These include the small features characterized by L_C' (gray) that continue to show a decreasing trend, while the large features characterized by L_C'' (open) show an increasing trend. These combined results in Fig. 6b suggest that increasing the glue concentration between 3 and 30 mg L^{-1} create smaller grains on the surface and, after a critical concentration, these features continue to grow as smaller grains but on top of much larger surface features. Similar conclusions can be made from the data in Fig. 6c when considering δ/L_C' as a function of glue concentration. At glue levels between 3 and 30 mg L^{-1}, there is a general increase in the height-to-width ratios and is most clearly observed in the inset. This occurs because the limiting roughness remains relatively constant, while the periodicity is decreasing. At glue concentrations of 37.5 and 60 mg L^{-1}, the data are again consistent with two distinct features on one surface. These correspond to very small features with a large δ/L_C' ratio that have been deposited on the underlying features characterized by a very small δ/L_C'' ratio. At first, these observations may seem counterintuitive. In the previous section, it was stated that glue may preferentially bind to protrusions on the surface that have a higher current density and forces deposition to occur in the valleys. This would result in an increasing grain size, which is in contrast with the current trends. However, the scaling analysis of the time-dependent study revealed that the smoothing mechanism was dominated by surface diffusion of zinc.

Therefore, as the level of glue is increased, one must also consider how the surface diffusion of zinc is affected. At very high levels of glue, zinc may not be able to diffuse across the surface to the same extent as at lower glue levels. Thus, the dominant smoothing mechanism could be hindered by excess levels of glue in the electrolyte. The extent to which this happens may be revealed by studying the values of α (black symbols) and α' (gray symbols) shown in Fig. 6d. The values of α show some fluctuations near 0.8 as the glue concentration is increased and therefore $n \sim 4$ under all conditions. This shows that the small features grow on the surface through a dominant mechanism of surface diffusion. At glue concentrations of 37.5 and 60 mg L^{-1}, the values of α' are extracted as 0.43 and 0.5, respectively. These values of α' describe the growth of the larger features and correspond to $n \sim 3$. This could be attributed to a growth mechanism associated with volume or bulk diffusion but could also be described by non-stochastic roughening by the creation of islands and/or nucleation on the surface [36, 37]. Moreover, these results are consistent with models that have included various grain sizes and shapes that are similar to the ones observed in the current study [46, 47], which further support the glue-induced changes in surface growth. As a final comment, the surfaces that contain both large and small zinc features were brittle and thus became difficult to remove from the aluminum surface without breaking.

4 Summary and conclusions

AFM, SEM, and scaling analysis were used to characterize the surface characteristics of industrially relevant zinc electrodeposits. In this study, the zinc deposits were produced on aluminum cathodes from an industrially relevant acidic zinc sulfate electrolyte containing various additives, including glue, and the current density was maintained at 44 mA cm^{-2}. Scaling analysis of the AFM images was used to determine the mechanism of surface growth and to extract surface features, including limiting roughness and periodicity (or grain size).

When the level of glue was maintained at 30 mg L^{-1} and the deposition time ranged between 10 and 90 min, the results show that growth is controlled by surface diffusion. Under these conditions, both the grain size and the limiting roughness of the surface were shown to increase as a function of deposition time but the grain size increased at a faster rate. These trends were used to predict the surface characteristics of zinc deposits that would be produced under the same conditions but at a longer deposition time. The analysis predicts that zinc samples produced after 48 h from these stated conditions will have values of $\delta \sim 4$ µm and $L_C \sim 36$ µm.

Further studies were performed on zinc deposits produced at a fixed deposition time of 30 min but from an electrolyte that contained a range of glue concentrations. The results show that small increments of glue (between 3 and 30 mg L^{-1}) cause a decrease in the grain size and an increase in the aspect ratio of surface features. However, after a critical concentration of 30 mg L^{-1}, the surface was characterized by two deposit morphologies on a single surface. These include large zinc deposits with smaller zinc features on their surfaces. Surfaces with these deposit morphologies were characterized with a unique scaling analysis plot that showed two distinct static exponents, α and α'. This was attributed to the competition of two deposit mechanisms, including surface diffusion and the formation of islands.

The combined results show how scaling analysis can be used to quantify the surface characteristics of zinc electrodeposits that are produced under industrially relevant conditions.

Acknowledgments This research was supported by Teck Metals Ltd. and the Natural Sciences and Engineering Research Council Canada (NSERC Engage and Engage Plus). We would like to thank Teck for granting approval to publish this research. Furthermore, we thank technicians Greg Lakanen and Henry Ylitalo of Laurentian University for machining the aluminum cathodes and Adam Walli for helping with some electrical components. We also acknowledge the Central Analytical Facility (CAF) of Laurentian University for the SEM analysis and Presley Hlushak (Teck) for sending samples, electrolytes, and additives.

References

1. Robinson DJ, O'Keefe TJ (1976) J Appl Electrochem 6:1–7
2. Dhak D, Mahon M, Asselin E et al (2012) Hydrometallurgy 111–112:136–140
3. Greul T, Gerdenitsch J, Commenda C et al (2014) Surf Coat Technol 253:8–13
4. Raeissi K, Saatchi A, Golozar MA et al (2004) J Appl Electrochem 34:1249–1258
5. Ping G, Pascual R, Shirkhanzadeh M et al (1995) Hydrometallurgy 37:267–281
6. Nusen S, Yottawee N, Daopiset S et al (2012) Hydrometallurgy 113–114:143–154
7. Pan J, Wen Y, Cheng J et al (2013) J Appl Electrochem 43:541–551
8. Beshore AC, Flori BJ, Schade G et al (1987) J Appl Electrochem 17:765–772
9. Dhak D, Asselin E, DiCarlo S et al (2010) ECS Trans 6:267–280
10. Saba AE, Elsherief AE (2000) Hydrometallurgy 54:91–106
11. Recéndiz A, González I, Nava JL (2007) Electrochim Acta 52:6880–6887
12. Torrent-Burgués J, Guaus E (2007) J Appl Electrochem 37:643–651
13. Díaz-Arista P, Meas Y, Ortega R et al (2005) J Appl Electrochem 35:217–227
14. Alfantazi AM, Dreisinger DB (2003) Hydrometallurgy 69:57–72
15. Trejo G, Ruiz H, Borges RO et al (2001) J Appl Electrochem 31:685–692

16. Aaboubi O, Douglade J, Abenaqui X et al (2011) Electrochim Acta 56:7885–7889
17. Nayana KO, Venkatesha TV (2011) J Electroanal Chem 663:98–107
18. Das SC, Singh P, Hefter GT (1997) J Appl Electrochem 27:738–744
19. Wu X, Liu Z, Liu X (2014) Hydrometallurgy 141:31–35
20. Gomes A (2006) da Silva Pereira MI. Electrochim Acta 52:863–871
21. Alfantazi AM, Dreisinger DB (2001) J Appl Electrochem 31:641–646
22. MacKinnon DJ, Brannen JM, Fenn PL (1987) J Appl Electrochem 17:1129–1143
23. Alkatsev VM, Alkatsev MI, Lin VA et al (2014) Metall Nonferrous Met 55:327–330
24. Mureşan L, Maurin G, Oniciu L et al (1996) Hydrometallurgy 43:345–354
25. Ivanov I (2004) Hydrometallurgy 72:73–78
26. Zhang QB, Hua YX, Dong TG et al (2009) J Appl Electrochem 39:1207–1216
27. Yu J, Wang L, Su L et al (2003) J Electrochem Soc 150:C19–C23
28. Boiadjieva T, Monev M, Tomandl A et al (2008) J Solid State Electrochem 5:671–677
29. Moats M, Guerra E, Gonzalez JA (2008) Zinc lead metallurgy. Canadian Institute of Mining, Metallurgy, and Petroleum, Montral, pp 309–314
30. Mackinnon DJ, Brannen JM (1977) J Appl Electrochem 7:451–459
31. Mackinnon DJ, Brannen JM (1986) J Appl Electrochem 16:127–133
32. Tripathy BC, Das SC, Hefter GT et al (1998) J Appl Electrochem 28:915–920
33. Khorsand S, Raeissi K, Golozar MA (2011) J Electrochem Soc 158:D377
34. Keist JS, Orme CA, Wright PK et al (2015) Electrochim Acta 152:161–171
35. Ballesteros JC, Díaz-Arista P, Meas Y et al (2007) Electrochim Acta 52:3686–3696
36. Williams RS, Tong WM (1994) Annu Rev Phys Chem 45:401–438
37. Zhao T, Zagidulin D, Szymanski G et al (2006) Electrochim Acta 51:2255–2260
38. Iwasaki H, Yoshinobu T (1993) Phys Rev B 48:8282–8286
39. Iwamoto A, Yoshinobu T, Iwasaki H (1994) Phys Rev Lett 72:4025–4028
40. Hiane M, Ebothé J (2001) Eur Phys J B 22:485–495
41. Nikolić ND, Rakočević Z, Djurovic DR et al (2006) Russ J Electrochem 42:1121–1126
42. Barasbasi A-L, Stanley HE (1995) Fractal concepts in surface growth. Cambridge University Press, New York
43. López JM, Castro M, Gallego R (2005) Phys Rev Lett 94:1–4
44. Saban MD, Scott JD, Cassidy RM (1992) Metall Trans B 23:125–133
45. Oniciu L, Mureşan L (1991) J Appl Electrochem 21:565–574
46. Oliveira TJ, Aarão Reis FDA (2011) Phys Rev Lett 83:1–7
47. Oliveira TJ, Aarão Reis FDA (2007) J Appl Phys 101:1–7